APRIL 01 2025

Humpback whale (*Megaptera novaeangliae*) breathing sound characteristics from simultaneous above and underwater measurements

Max K. Radermacher ; Matthew E. Schinault ; Sai Geetha Seri ; Hamed Mohebbi-Kalkhoran ; Nicholas C. Makris ; Purnima Ratilal

J. Acoust. Soc. Am. 157, 2304–2318 (2025)
https://doi.org/10.1121/10.0036353

JASA ARTICLE

Humpback whale (Megaptera novaeangliae) breathing sound characteristics from simultaneous above and underwater measurements

Max K. Radermacher,[1,a)] Matthew E. Schinault,[1] Sai Geetha Seri,[1] Hamed Mohebbi-Kalkhoran,[1] Nicholas C. Makris,[2] and Purnima Ratilal[1]
[1]Department of Electrical and Computer Engineering, Northeastern University, Boston, Massachusetts 02115, USA
[2]Department of Mechanical Engineering, Massachusetts Institute of Technology, Cambridge, Massachusetts 02139, USA

ABSTRACT:
Humpback whale breathing-related sounds were recorded on elements of a coherent hydrophone array subaperture deployed vertically at the Great South Channel on the US Northeastern continental shelf in Fall 2021, where half of the hydrophones were in-air and the rest submerged underwater. In-air hydrophones recorded breathing sounds w approximately 2.5 s duration, but smaller bandwidths compared to underwater hydrophones where signal energies extended beyond 50 kHz, and a mean underwater source level of 161 6 4 dB re 1 lPa at 1 m, based on measurements at 22.9 m. The underwater recorded humpback whale breathing sound spectra displayed a broadband dip centered 15.7 kHz, with approximately 400 Hz half-power bandwidth, likely caused by attenuation from propagation through pulsating air bubbles. The air bubble radius for natural frequency of oscillations at 15.7 kHz is estimated to be 0.205–0.21 mm. These bubbles are capable of removing energy from the forward propagated humpback breathing sounds via resonance absorption most pronounced at and near bubble natural oscillation frequency. Humpback wha distances from the vertically deployed hydrophones are estimated and tracked by matching the curved nonlinear travel-time wavefront of its breathing sounds, since the whale was in the near-field of the subarray.
 https://doi.org/10.1121/10.0036353
(Received 29 October 2024; revised 10 February 2025; accepted 11 March 2025; published online 1 April 2025)
[Editor: Aaron M. Thode] Pages: 2304–2318

I. INTRODUCTION

Humpback whales (Megaptera novaeangliae), a species belonging to the baleen whale (Balaenopteridae) family (Clapham, 2000; Erbe, 2002), produce an assortment of sounds ranging from vocalized moans and songs to dynamical surface-breaching, breathing and foreflipper flaps. Humpback whales breathe through their two blowholes located at the top of their head. The air is carried from their blowholes down their nasopharynx, and eventually reaching a thick ridge of tissue, known as the u-fold. The u-fold is an important aspect in the sound production and breathing mechanism for baleen whales. The u-fold resembles the lips on a human, which is capable of opening and closing and resides alongside the laryngeal sac (Cazau et al., 2016; Damien et al., 2019). Air which is held in the laryngeal sac, is moved to and from lungs through the contraction and expansion of muscles. When air is moved back and forth between the sac and lungs, it must pass by the u-fold, creating vibrations. Audible sound is produced from the force and muscle exertion used to move air from the laryngeal sac to the lungs and eventually expelled through the blowholes. These sounds can be generated through breathing, as a way of communication (Gandilhon et al., 2015; Reidenberg and Laitman, 2007b). The analysis of this paper focuses on the former. A humpback whale surface breathing spray or blow can be described as a balloon or bushy shaped blow that is typically 2–3 m high (Leatherwood et al., 1982), with a mean blow velocity ranging from 13 to 23 km/h (Horton et al., 2017). Blows are a mixture of seawater, exhaled gases, and intrinsically generated aerosol droplets (Yeates et al., 2020). Using a mean length of 10.1 6 3.8 m for a female humpback whale (Reidenberg and Laitman, 2007b), with a whale length to lung capacity ratio derived in Krogh (1934), the whale can expel a mean of 5200 6 1900 liters of air (5.2 6 2.0 m^3 lung capacity) per blow. Although Krogh (1934) derived the lung capacity for a blue whale, it is considered to be a rough estimate after correcting for the size difference. Humpback whales have a distinct characteristic, unlike other baleen whales according to Reidenberg and Laitman (2007a), in that they expel large amounts of air underwater, creating a bubble cloud or wall. Images of humpback whales can be seen in Fig. 1 with surface breathing sprays in Fig. 1(b) and underwater bubble cloud in Fig. 1(c).

The humpback whale breathing sound signals analyzed here were acquired using a coherent hydrophone array subaperture during an experiment in the Great South Channel

a)Email: radermacher.m@northeastern.edu

https://doi.org/10.1121/10.0036353

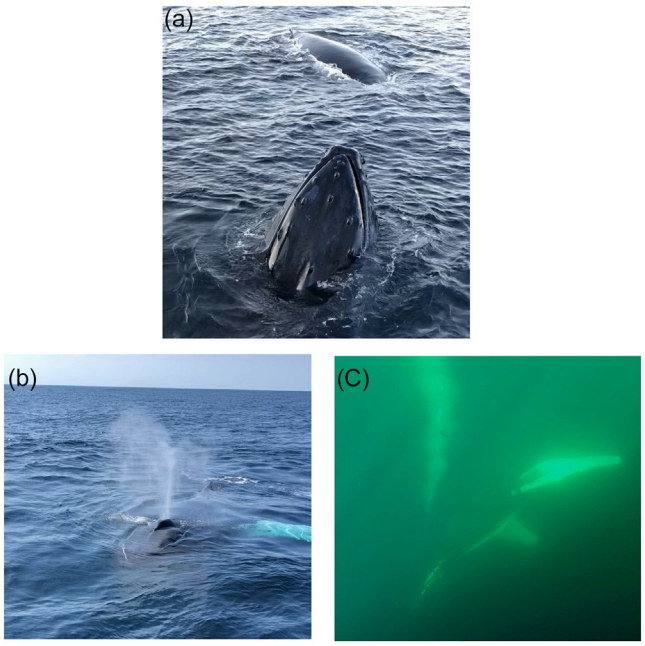

FIG. 1. (a) Two humpback whales, three meters off the starboard side of RV Endeavor, photographed on Monday September 6, 2021 at 20:07 EDT at the Great South Channel; (b) humpback whale surfacing on Monday September 6, 2021 at 20:00 EDT; and (c) humpback whale blowing bubble cloud under the port side of the boat on Wednesday September 8, 2021 at 15:04 EDT, photographed using GoPro.

(GSC) of the U.S. Northeast continental shelf (Fig. 2) in Fall 2021. The large-aperture densely populated coherent hydrophone array system, capable of digitizing acoustic data with a sampling frequency up to 100 kHz, was designed and fabricated in-house at Northeastern University (NU) (Mohebbi-Kalkhoran et al., 2022; Radermacher et al., 2022; Schinault et al., 2022). The array system can be deployed in both drifting vertical and towed horizontal modes, and we present recordings of humpback whale breathing sounds in both configurations. The coherent hydrophone array has been effective for instantaneous, wide-area detection, classification, and localization of marine mammal vocalizations including humpback whale songs and social moan calls in past experiments, where data were analyzed using the passive ocean acoustic waveguide remote sensing (POAWRS) technique (Huang et al., 2016; Ratilal et al., 2022; Wang et al., 2016), leading to a multifaceted and extensive list of uses: from monitoring marine biodiversity and ecology (Garcia et al., 2019; Wang et al., 2016) to man-made objects, such as ship radiated sounds (Zhu et al., 2020), to rain and other geophysical processes (Wilson and Makris, 2006, 2008).

Humpback whale moans and songs have been extensively recorded and studied previously (Huang et al., 2016; Noad et al., 2000; Payne and McVay, 1971; Winn and Winn, 1978), but there are limited recordings and studies on humpback whale breathing sounds. In Watkins (1967), humpback whale blows were categorized into two types; ordinary/normal blows and wheezing blows. Wheezing blows are believed to be voluntarily made and can be heard both in-air and underwater, unlike ordinary blows which can be heard only in-air. During Watkins 1961 experiment off Cape Cod, the underwater hydrophone and in-air microphone recording systems had flat responses from 50 Hz to 10 kHz, but spectrograms were only shown up to 4 kHz. Both the wheezing and ordinary blows recorded an upper frequency value of 2 kHz, where the wheezing blow had about 35 dB louder sound that lasted around 2 s, almost twice that of the ordinary blow. Here, our recordings of humpback whale breathing sounds are sampled at 100 kHz, a factor of 12.5 times higher sampling rate than the measurements of Watkins (1967). This higher sampling rate is essential for capturing a fuller bandwidth for the humpback whale breathing sound signals, especially underwater.

The humpback blows were also analyzed by Thompson et al. (1986) and categorized as shrieks and trumpetlike hum blasts, where the shrieks had a maximum frequency of 2 kHz, and the blasts with a mean frequency of 114 Hz. Thompson et al. (1986) shows humpback whale blow sound

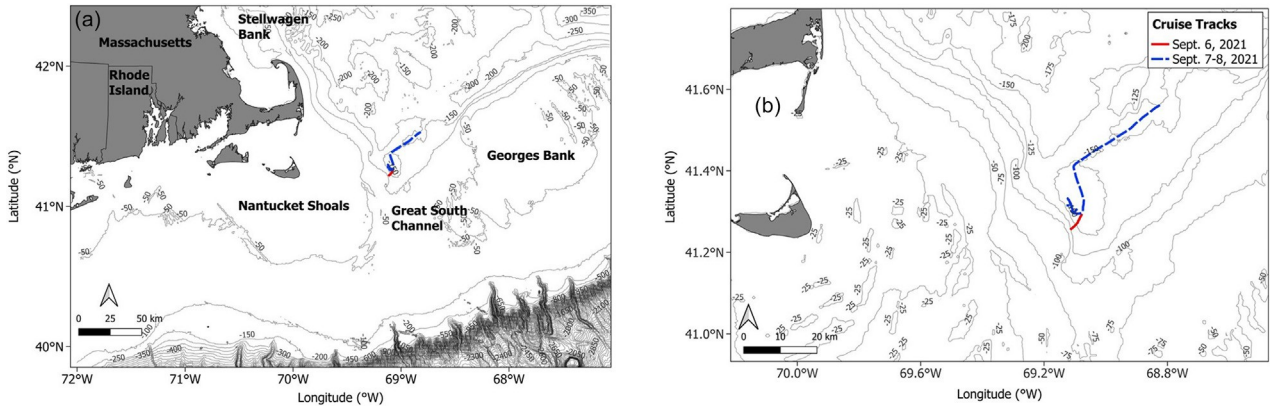

FIG. 2. (a) Experimental region where subapertures of a 160-element coherent hydrophone array were deployed from September 6–8, 2021. (b) Close of the research vessel tracks at the Great South Channel acquiring data, where the (solid) red track shows locations of the array in vertical drift mode September 6, 2021 and the (dashed) blue track is where the array was horizontally towed on September 7–8, 2021. Images generated with QGIS System Software.

spectrograms with a wider bandwidth of up to 8 kHz than that of Watkins (1967). Thompson et al. (1986) accredits the sequence of these sounds to a form of communication or encounter with social significance, where the estimated source level for shrieks range from 179 to 181 dB re 1 μPa at 1 m, and blasts range from 181 to 185 dB re 1 μPa at 1 m. There are some distinct frequency and source level differences between song and non-song humpback whale calls, providing some insight into the range threshold detection of different sounds (Au et al., 2006). Recording and classifying these breathing sounds help gain a deeper understanding of humpback whale communication, including the ways they interact and signal each other above the water surface.

The humpback whale surface breathing activities generate blows and sprays that entrain air bubbles at the sea surface, as well as from breaking waves due to dynamical body motions. Likewise, their underwater blows also generate bubbles. Here, we examine the impact of humpback breathing-related or underwater bubble generation and compare it to other mechanisms that generate bubbles in the ocean, in particular, precipitation and wind-dependent breaking waves. Rainfall is a source of significant underwater sound and the characteristics of the sound is dependent on the rainfall rate, drop size and terminal velocity which has been investigated in Barclay and Buckingham (2013a), Ma et al. (2022), Ma and Nystuen (2005), Medwin (1977), Nystuen (1992), Pumphrey and Crum (1990), Pumphrey et al. (1989), Pumphrey and Elmore (1990), and Pumphrey and Walton (1988).

Small raindrops (0.8–1.1 mm diameter) produce a distinct broadband peak in the spectra around 15 kHz, a sound characteristic of drizzle and light rain, where the total rainfall rate is less than 2.5 mm/h (Medwin et al., 1992; Nystuen et al., 1993). Medwin et al. (1992) demonstrates the correlation between drop size and bubble radius, where small raindrops produce an underwater bubble radius of approximately 0.217 mm. Pumphrey and Elmore (1990) associate that radius to a natural frequency of roughly 15 kHz. Medium to heavy rainfall have higher sound spectral levels than drizzle and light rainfall, and decay roughly monotonically with increasing frequency out to 50 kHz with no distinct peaks (Anagnostou et al., 2008). Similar to rainfall, breaking waves are a source of underwater sound that varies depending on wind speeds and wave height. This phenomenon was investigated in Deane and Stokes (2002), where the acoustic phase of a breaking wave lasts approximately 1.2–1.5 s, with a broad bandwidth and a spectral peak below 1 kHz.

Here, we analyze humpback whale breathing sounds recorded simultaneously in-air and underwater, providing time-series and power spectral density (PSD) analysis. Comparing these measurements provides insights and key differences between in-air and underwater recordings. Whale ranges from the receiver array are estimated from the underwater recorded humpback breathing sounds by modeling the nonlinear curvature of the acoustic wavefront, due to their close proximity in the near-field of the submerged hydrophone subarray. These localization results are employed to estimate the source level distribution for underwater recorded humpback breathing sounds, which are then compared to those published in Dunlop et al. (2013) and Thompson et al. (1986). Finally, the underwater recorded humpback breathing sound PSDs are compared to those generated by geophysical processes such as precipitation and breaking waves, to provide an understanding and further insights into humpback breathing-related sound effects.

II. MATERIALS AND METHODS

A. Experiment and data collection

The data analyzed here is a subset drawn from the U.S. Northeast coast 2021 experiment (Schinault et al., 2022) conducted on the research vessel Endeavor while at the GSC, a region beginning less than 50 NM east of the Nantucket Shoals, from September 6–8, 2021. Humpback whale breathing sounds were recorded on a 32-element subaperture of a densely populated coherent hydrophone array deployed in two configurations, vertical drift and horizontal tow. One of the most prominent species, captured both acoustically and on video, was the humpback whale. Periods occurred where dozens of humpback whales surrounded the boat, so the array could not be towed for those time periods. This became an opportunistic time period to deploy a 32-element HF (high frequency, with roughly 0.375 m interelement spacing) subaperture of the array vertically in drift mode. In this configuration, hydrophones 1–13 were consistently in-air, 14–17 transitioned between in-air and underwater due to surface waves, and hydrophones 18–32 were consistently underwater. During vertical deployments, spectrograms of the recorded data were generated for each hydrophone individually, encompassing both in air and underwater measurements.

When the array was towed subsequently, 16 hydrophones were used for beamforming, providing an enhancement in signal-to-noise ratio (SNR), that leads to an increased detection range and improved signal quality. In this experiment, beamformed spectrograms were generated in near-real-time spanning all 360° azimuths about the receiver array. The beamformed spectrograms captured a variety of vocalizations from marine mammal species, such as humpback songs, fin whale 20 Hz pulses, minke whale boing sequences, orca and other delphinid whistles, as well as sperm whale and other delphinid echolocation clicks in the 10 Hz to 50 kHz range (Seri, 2024). Other signals present in the beamformed spectrogram imagery include fish grunts and knocks, and ship-generated tonal, broadband, and transient sounds. The POAWRS technique typically detects hundreds of thousands to several million acoustic signals per day, in the 10 Hz to 50 kHz frequency range when deployed in biodiverse hotspots (Garcia et al., 2020). Here, we focus our analysis specifically on humpback whale breathing sounds.

Concurrent in-air and underwater hydrophone recordings of whale breathing sounds were acquired across a 40

https://doi.org/10.1121/10.0036353

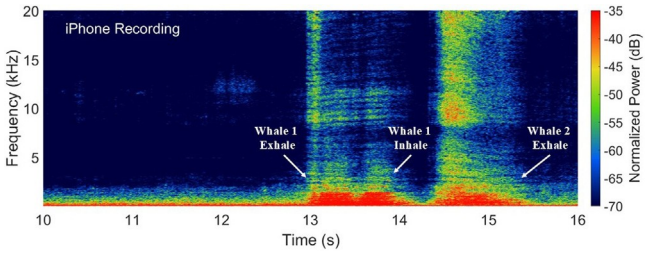

FIG. 3. Spectrogram from iPhone video recording of several humpback whale breathing sounds on September 6, 2021, at 18:06 EDT in the Great South Channel.

minute time interval from 20:29 EDT to 21:09 EDT containing 274 breaths on September 6, 2021, where the array was deployed vertically. Video recordings were leveraged to help aid in narrowing in on specific time windows. This proved to be quite crucial when identifying the spectrograms for humpback whale breaths, both above and below the surface of the water. On September 6, 2021 at 18:06 EDT, an iPhone video captured multiple whales surfacing adjacent to the boat. This recorded video was converted into a Waveform Audio File Format (WAV) in MATLAB, which was then used to generate a spectrogram as seen in Fig. 3, with the full video included as supplementary material. This spectrogram, along with other visual sightings and video recordings were used to coregister sounds recorded on individual hydrophones of the subarray. It was pertinent to have a template to be able to manually classify spectrograms as humpback whale breathing sounds, which were originally documented as unknown acoustic signals.

B. PSD estimation of humpback whale breathing sounds measured on a coherent hydrophone subarray

PSD analysis demonstrates the power distribution across a signal's frequency range. The PSDs are first calculated via Fourier transform analysis for individual whale breathing sound signals, which were then combined to calculate the time averaged power spectrum. The PSDs are calculated separately for the three configurations; individual in-air and underwater hydrophones in vertical deployment mode, and beamformed signal while the array was towed. All in-air measurements were normalized to their peak because of the unknown in-air hydrophone sensitivities due to the change in acoustic medium. In contrast, results of underwater power spectra are converted to dB re 1 μPa^2/Hz after correcting for known hydrophone sensitivities. It is important to note that the sound transmission between both mediums was not considered, given the unknown in-air sensitivity for the hydrophones. Where, on average, for a flat surface, the transmission loss is approximately 30 dB, which can vary depending on several parameters, such as surface roughness and frequency (Godin, 2007, 2006, 2008a,b; McDonald and Calvo, 2007).

C. Range estimation of humpback whale breathing sounds

Here, we estimate the range of humpback whales from the receiver subarray by employing time difference of arrival of the breathing sounds received on individual unmerged hydrophones. Due to the close proximity (less than 25 m), based upon visual sightings of the humpback whales in the near-field of the subarray, the received breathing sound wavefronts are curved. By utilizing the nonlinear travel time information, range estimation of the whales will be solved as a least squares cost function optimization problem.

The underwater hydrophones utilized in the range estimation were 24–28, 30, and 32, due to their location away from the hull of the boat. The setup is modelled in Fig. 4 showing the vertical array deployment. Let h be the depth of the first shallowest hydrophone from the sea surface used in the analysis and the depth of the nth hydrophone is $z_n = h + Dz_n$, where Dz_n is the separation of the nth hydrophone to the first. Let, z_w be the depth of the whale from the sea surface. The whale is assumed to be on the surface of the water, but the mechanism for creating sound in the whale is assumed to be slightly below the surface of the water. Due to this, a value of 1 m was assumed for z_w.

The difference in the distance, a_n, the sound needs to travel between the first element (hydrophone 24), r_1, and each subsequent element, r_n, is

$$a_n = r_n - r_1 = (Dt_n) c; \quad (1)$$

where c is the sound speed assumed to be 1500 m/s and Dt_n is the measured time-delay in seconds between the nth and first elements. The distance the sound needs to travel to the first element is

$$r_1 = \sqrt{x^2 + (h - z_w)^2}; \quad (2)$$

where x is the unknown horizontal range of the whale from the subarray. Each of the subsequent elements calculated distance is given by

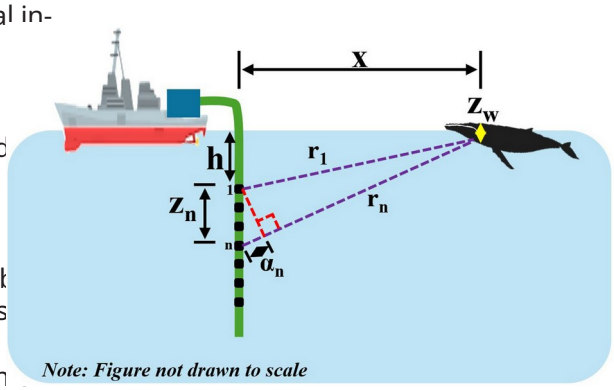

FIG. 4. Schematic of the subarray's vertical deployment underwater, showing the geometry used to formulate the equations needed to estimate whale horizontal range x.

$$r_n = \sqrt{x^2 + (h + \Delta z_n - w)^2}. \quad (3)$$

In order to determine values for x and h, a grid search from 0 to 50 m for x and 0 to 25 m for h, both with a step size of 0.1 m was used. The constraints of the grid were determined based upon visual sightings for x and known inter-element spacing for h. A least squares cost function was used as an optimization technique, where the optimized solution is the minimum of the function. The equation used for the cost function optimization is

$$\text{Cost} = \sum_{n=1}^{N} a_n (r_n - r_1)^2, \quad (4)$$

where N is 7, the total number of hydrophones analyzed. This optimization technique was applied across a subset of data to determine a series of humpback whale horizontal range estimates from a sequence of their measured breathing sounds. Forty-minutes of data were analyzed on September 6, 2021, from 20:29 EDT to 21:09 EDT, where the array was deployed vertically.

D. Focused near-field beamforming of humpback whale breathing sounds on vertical subarray

Two separate beamforming methods are utilized here to combine data from multiple elements of the submerged hydrophone subarray, focused near-field beamforming and traditional far-field beamforming. The focused beamform analysis uses data from seven underwater hydrophones 24–28, 30, and 32 during vertical drift deployments and employs the measured curved non-linear travel time-delay between elements and known inter-element spacings. A Hanning window function is applied across the hydrophones in the beamforming. The far-field beamformer follows a similar approach but uses a linear travel time-delay instead due to plane wave assumption. Beamforming with data from an array of hydrophones typically enhances the SNR over measurements of a single hydrophone, especially true for large horizontal arrays, since they filter out signals and noise from all other bearings, except for the steered direction (Garcia et al., 2019; Wang et al., 2016). Here, the subarray is deployed vertically and only 7 hydrophones are used, we will examine the beamformed result for potential enhancements.

E. Source level estimation of humpback whale breathing sound

The source level (SL) of each humpback whale breathing sound during underwater vertical deployment in units of dB re 1 μPa at 1 m was estimated from its respective received pressure level (RL) by accounting for one-way transmission loss, where Seriet al. (2023) took a similar approach. Using the equations derived in Francois and Garrison (1982) for absorption, and the transmission equation provided in Sec. 5.3 of Urick (1983), the following equation was implemented:

$$TL = 20 \log_{10}(r) + \alpha(f) r 10^{-3}. \quad (5)$$

Here, TL is the transmission loss in dB re 1 m, r is the distance in meters, α(f) is the frequency dependent absorption coefficient in dB/km, where 10^{-3} is required for conversion from meters to kilometers. Due to the broad bandwidth of the humpback breathing sound, the absorption coefficient was integrated across the frequency range. Here, SL = RL + TL, and RL = $20 \log_{10}(|P|/P_{ref})$, where P is the sound pressure level of the whale breathing sound, and P_{ref} is the reference sound pressure, 1 μPa. This equation assumes no bubbles or other inhomogeneities are present, and due to the close proximity of the whale, the source level could be approximated by strictly considering spherical spreading loss, verified by the absorption parameter accounting for less than 0.1 dB. Given whale location at the sea surface, it is important to determine if the whale acted as a dipole or monopole source. Due to the whale being right at the surface of the water and not below it, no mirror reflections from the air-water interface were observed. This was validated by comparing the RL at different depths where the mean and standard deviation were 137.4 ± 0.7 dB re 1 μPa, and the RL for each hydrophone are random deviations, and not following a deterministic trend as would be observed for a dipole source with directional beampattern. The whale breathing sound time domain signals were high-pass filtered to remove ship tonals, and then a band-stop filter was applied to filter-out the echosounder signal.

III. RESULTS

A. Humpback breathing sound bandwidth and signal duration

Subapertures of the coherent hydrophone array recorded humpback whale breathing related sounds from September 6–8, 2021, with majority recorded while the array was deployed in vertical drift mode on the sixth. The array also captured humpback breathing sounds in the late morning on the eighth while the array was being towed. This led to three distinct measurement scenarios: in-air and underwater subarray recordings during vertical drift deployments, and fully submerged subarray beamformed results during horizontal tow. These three measurement scenarios resulted in significantly distinct spectrograms and spectra due to differences in recorded humpback breathing sound signal bandwidth, duration and intensity.

The comparison between concurrent in-air and underwater hydrophone recordings during vertical drift deployment can be made from Fig. 5, with the full videos included as supplementary material. The spectrogram of an underwater hydrophone recording during vertical deployment shows four distinct humpback whale breathing sounds in Fig. 5(a). The gray (background noise) and magenta (signal with background noise) bounding boxes show the duration and

JASA
https://doi.org/10.1121/10.0036353

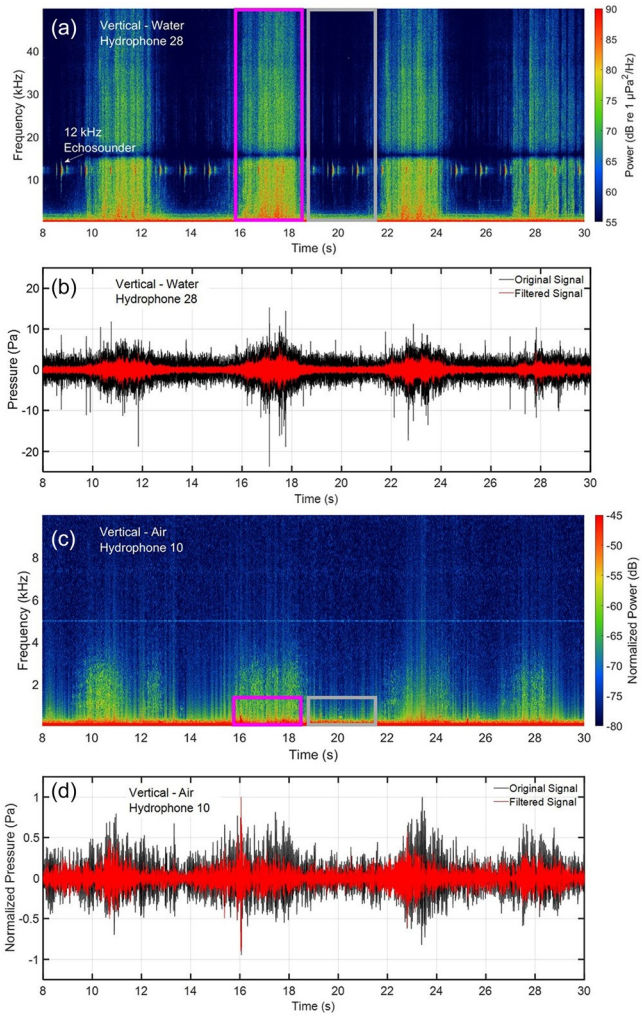

FIG. 5. (a) Spectrogram of measurement from underwater hydrophone 28 during vertical deployment showing several recorded humpback whale breathing sounds; (b) time-series analysis of underwater hydrophone 28 measurement, including result after bandpass filtering with cut-off frequencies set at 300 and 10 kHz (red); (c) spectrogram of measurement from in-air hydrophone 10 during vertical deployment showing several recorded humpback whale breathing sounds; (d) time-series analysis of in-air hydrophone 10 measurement, including result after bandpass filtering with cut-off frequencies set at 30 Hz and 1.2 kHz (red). All plots recorded on September 6, 2021 at 20:53 EDT, with the array being deployed vertically.

frequency range included in calculating their respective power spectrum. A consistent broadband frequency notch dip centered at 15.7 kHz was observed in recordings of all underwater hydrophones during vertical deployment and will be discussed further in Sec. IV. The corresponding time-series is shown in Fig. 5(b), where the filtered time-series (in red) has low frequency ship tonal and high frequency echosounder pulses removed via a 300 Hz to 10 kHz bandpass filter. The spectrogram of concurrently recorded humpback whale breathing sounds on an in-air hydrophone is shown in Fig. 5(c), showing a significantly smaller frequency bandwidth than the underwater case, mainly due to higher acoustic attenuation in-air versus water and location of in-air hydrophone. The corresponding in-air time-series of the recording is shown in Fig. 5(d), where the filtered time-series (in red) is obtained from the normalized signal after bandpass filtering over 30 Hz to 1.2 kHz, capturing the breathing sound bandwidth for air and filtering out the low-frequency noise.

The power spectra for humpback breathing sounds and background noise are calculated using signal time-series subsets within the same data file. Examples are shown in Figs. 5(a) and 5(c) for an underwater and an in-air hydrophone, respectively, with a pink bounding box demarcating humpback breathing sound segments and a gray bounding box demarcating noise segments. The spectra are plotted in Fig. 6, where the results are time-averaged across 20 distinct humpback breathing sound and corresponding noise segments. Background noise is computed in the absence of humpback breathing sounds but residual bubbles remain, leading to a broadband dip of 15.9 6 0.6 kHz with an intensity value of 41.3 6 2.9 dB. The spectra are based on individual hydrophone recordings with a 5 Hz running average applied. Both log-scale and linear frequency scales are used in the plots to provide a clearer comparison in signal versus noise spectral amplitudes, especially at low frequencies, allowing for a more accurate determination of bandwidth. The underwater humpback breathing sound signal has frequency components extending beyond 50 kHz as can be seen in Figs. 5(a) and 6(c). The large spectral peak at about 12 kHz seen in Figs. 6(c) and 6(d) was caused by the ship's onboard EDO UQN 323C transducer (echosounder), which occurred during the entire vertical drift deployment with an approximate 1-s inter-pulse interval. There is no evidence to suggest the 12 kHz echosounder is creating the broadband frequency dip. Two explanations support this conclusion: (1) the dip is not periodic but rather constant and (2) the echosounder is a mechanical acoustic source radiating independently from the whale and therefore not generating waves to coherently interfere with whale breathing sound. A power spectrum showing humpback breathing sounds in the absence of echosounder signals can be seen in Fig. 12(b), where the acoustic data segments are taken from intervals between echosounder pings. The echosounder signal was ignored when determining the energy of humpback breathing sound in underwater hydrophone measurements during vertical drift deployment.

Sixty-six hydrophone elements were utilized to generate the beamformed spectrogram in Fig. 7 for the horizontally towed subarray case where the humpback breathing sound was located at 80.1 bearing relative to array heading, where 90 corresponds to forward endfire (towards ship). In both the in-air and underwater vertical deployments, the signal duration was 2.5 s, while for the towed case, it is only roughly 1 s in duration, which will be discussed further in Sec. IV. In addition, due to the humpback whale breathing sound being low in intensity compared to the background noise during the horizontal configuration, it was difficult to detect and manually classify the sounds. Background noises can consist of a wide variety of sounds, including biological noise (Cato, 1978, 1992), flow noise (Auvinen et al., 2020), and wind-generated noise

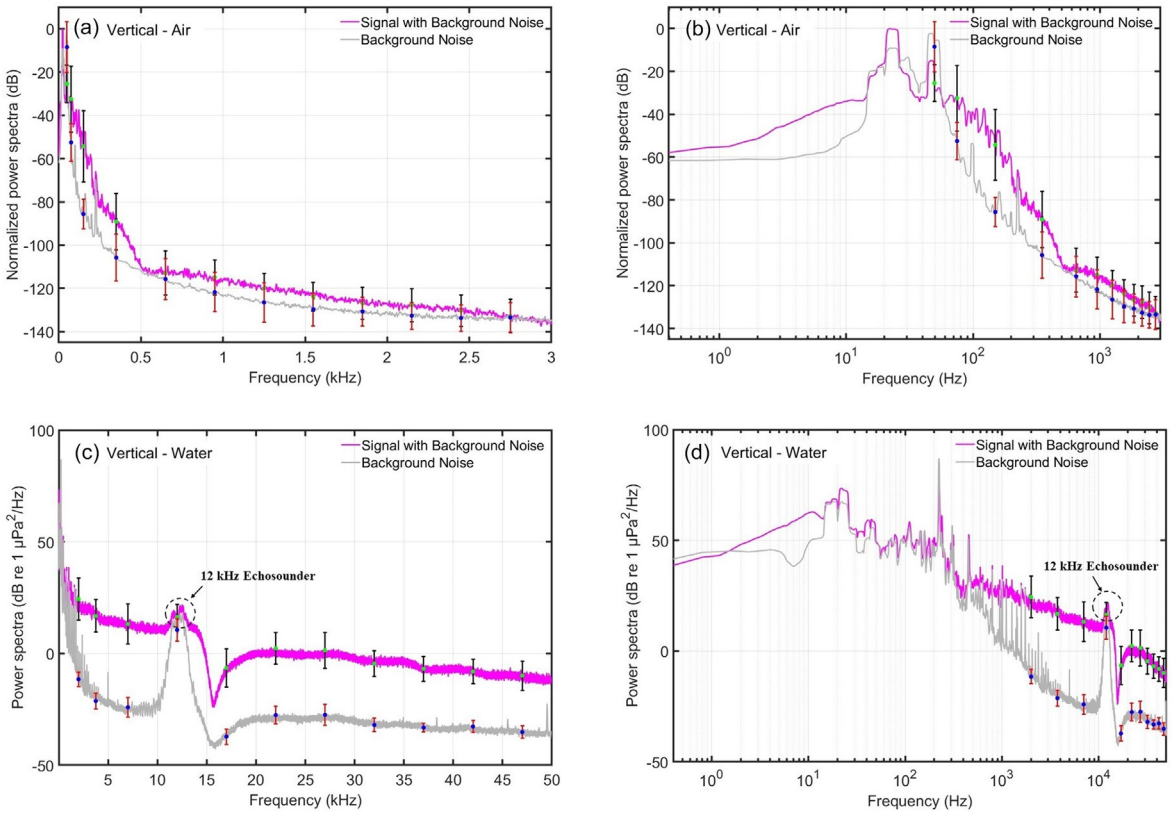

FIG. 6. Average power spectrum of 20 humpback whale calls and background noise region with array deployed vertically. (a) In-air measured power spectrum with linear frequency-axis; (b) in-air measured power spectrum with log-scale frequency-axis; (c) in-water measured power spectrum with linear frequency-axis; (d) in-water measured power spectrum with log-scale frequency-axis.

(Barclay and Buckingham, 2013b). The 3 dB frequency bandwidths for humpback breathing sound in each measurement scenario is tabulated in Table I.

B. Humpback whale range estimation from near-field breathing sounds measured on vertical array subaperture

The waterfall plot [Fig. 8(a)] shows the time-series and hence time-delay for a humpback breathing sound signal received on the seven underwater hydrophones analyzed here. Matched filtering [Fig. 8(b)] was used to provide more accurate time-delay estimates across the hydrophones. Here, the signal from hydrophone 28 was used as the model signal for each humpback whale breathing sound by applying a time reversal to its time-series. This time-reversed signal is then convolved with each of the seven individual hydrophone data, where the resultant is used due to its ability to create sharp peaks, leading to a more defined and accurate time-delay measurement.

The humpback breathing sound signals from multiple whale individuals were recorded at a rate of roughly 6.85 breaths per minute during vertical drift deployment on September 6, 2021. Fifteen humpback breathing sounds were analyzed individually to estimate sequence of whale horizontal ranges, x, and depths of first element (hydrophone 24), h. Figure 8(c) shows the measured, $\Delta r_n = \Delta t_n c$, versus calculated, $\Delta r_n = r_n - r_{n-1}$, relative travel distances for a

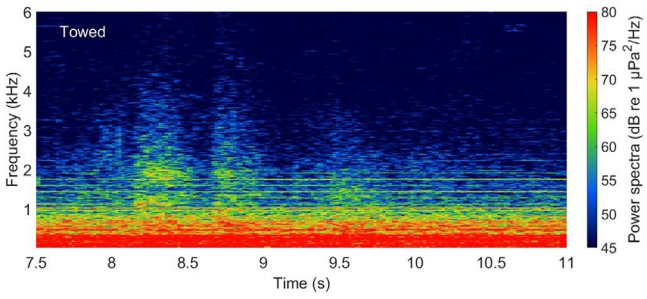

FIG. 7. Spectrogram of humpback whale call at relative bearing 0.89, equating to 80.1°, where 90° corresponds to forward endfire (towards ship) while the array is being towed on September 2, 2021 at 11:41 EDT (full video included as supplementary material).

TABLE I. Frequency bandwidths for measurements in the three distinct configurations of humpback whale breathing sounds.

Configuration	Sound type	f_{LOW} (kHz)	f_{HIGH} (kHz)	f_{BW} (kHz)
Vertical: Air	Infrasound	0.004	0.012	0.008
Vertical: Air	Audible/Ultrasound	0.070	0.400	0.330
Vertical: Water	Infrasound	0.005	0.012	0.007
Vertical: Water	Audible/Ultrasound	0.700	>50	>49.3
Towed	Audible/Ultrasound	1.000	3.750	2.7500

https://doi.org/10.1121/10.0036353

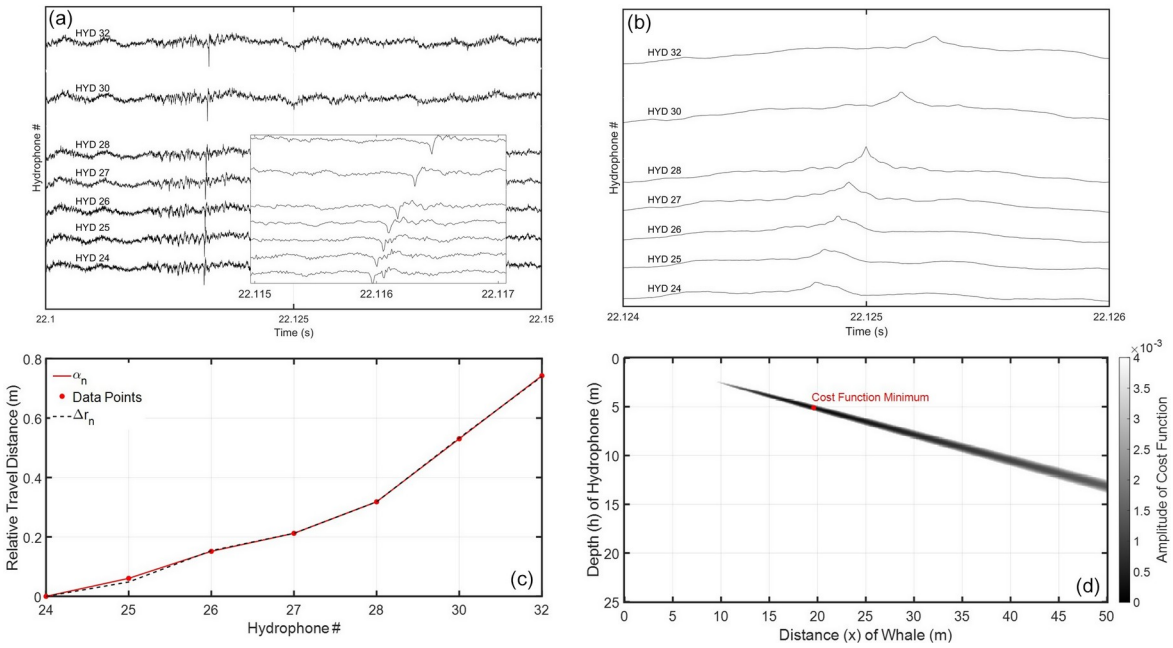

FIG. 8. (a) Waterfall plot of time series containing a humpback whale breathing sound recorded on September 6, 2021 at 20:53 EDT measured by seven underwater hydrophones deployed vertically. (b) Match filtered result of the given time series where data from hydrophone 28 is employed as the filt Calculated versus measured relative travel distances, with respect to the first hydrophone (hydrophone 24) analyzed; (d) the least squares cost functio mum showing estimates for x and h.

received humpback breathing sound signal. The calculated travel distances to the individual hydrophones relative to t first element (hydrophone 24) were obtained from Eqs. (2) and (3) using the x and h parameter values at the least squares cost function global minimum in Fig. 8(d).

Each measured humpback whale breathing sound resulted in a calculated x and h value. Due to surface wave each h value corresponding to the depth of the first eleme (hydrophone 24) varied slightly. The average h value is 3.9 m and this result is consistent with visual observations The horizontal distance, x, estimates of the received humpback breathing sound signals across the analyzed time du tion is shown in Fig. 9(a), having a mean of 16.2 m, a minimum of 9.1 m, and a maximum of 22.9 m. These resu demonstrate a strong correspondence with sighti ings and were used to estimate source level values as seen in F 9(b). The error bars are calculated from the 3 dB bandwidt of their respective least-squares cost function minimum, which shows the potential distance estimation errors.

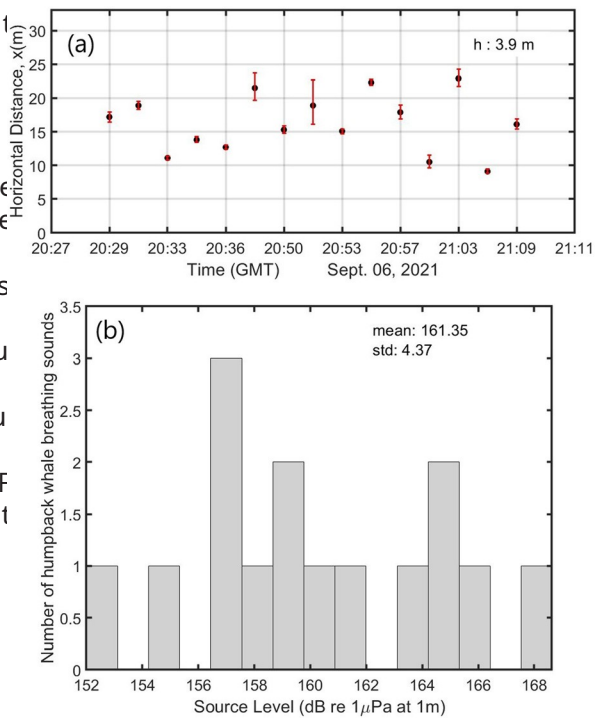

FIG. 9. Humpback whale breathing sounds recorded during horizontal drift deployment on September 6, 2021 from 20:29 EDT to 21:09 EDT. (a) Fifteen humpback whale horizontal distance values, x, vary from 9.1 to 22.9 m with an average of 16.2 m. The (red) error bars are calculated from the 3 dB bandwidth of the cost function minima, showing the potential range estimation errors. (b) Histogram of 15 humpback whale breathing sound source level estimates ranging from 152 to 168.7 dB re 1 lPa at 1 m with a mean and standard deviation of 161.6 4 dB re 1 lPa at 1 m, and mode or most probable value of 157 dB re 1 lPa at 1 m.

C. Focused beamforming of subarray underwater data during vertical drift deployment

Data from hydrophone 28 was compared with near-field and far-field beamforming results. These spectrograms were normalized to their respective peak intensity value which was calculated between the frequency range of 700 Hz to 4 kHz, during a 3-s time duration. Both beamformed results have lower noise halos surrounding the humpback whale breathing sounds in the spectrogram, compared to the single-hydrophone result. Since the differences with the

beamformed results are only marginal, the rest of the analysis uses data from a single hydrophone.

D. Source level distribution for humpback whale breathing sounds measured underwater

The received pressure level (RL) of humpback whale breathing sounds measured on submerged hydrophone 28 while deployed in vertical drift mode ranged from 131 to 141.6 dB re 1 μPa. With the humpback whale floating on the surface of the water, and with hydrophone 28 at known depth of 5.245 m, the transmission losses (TL) from whale locations to hydrophone locations were first calculated and averaged across a range of frequencies over the whale breathing sound bandwidth. The TL corrections were next applied to the measured RL, where mean transmission loss value was 24.5 dB re 1 m. The 15 source level estimates of whale breathing sounds range from 152 to 168.7 dB re 1 μPa at 1 m, as seen in Fig. 9(b). The mean and standard deviation for humpback whale breathing sound source level distribution are 161 ± 4 dB re 1 μPa at 1 m, with a mode or most probable value of 157 dB re 1 μPa at 1 m.

IV. DISCUSSION

We applied visual sightings and video recordings to identify and coregister humpback whale breathing sounds recorded on individual elements of a coherent hydrophone subarray during vertical drift deployment and to beamformed results during horizontal tow. The 1 s duration of humpback breathing sounds in beamformed spectrograms of subarray horizontal tow measurements is smaller than the 2.5 s duration measured by the hydrophone elements during vertical drift deployment. This is because the hydrophones in vertical drift are much closer to the humpback whales and in the near-field distance, while hydrophones in horizontal tow are further away and in the far-field distance to the whale sounds. Close inspection of humpback breathings sounds in Fig. 5(a) from vertical deployment show that each 2.5 s duration signal is dominated by two to three highly energetic segments of roughly 1 s duration and these energetic segments are the only sounds that stand above the background noise during horizontal tow. The in-air hydrophone spectrograms during vertical drift deployment show a smaller frequency bandwidth than that from the iPhone video recording. This is because during the iPhone recording, the humpback whales were adjacent (less than 3 m) from the boat, while the whales were on average 16.2 m away from the array during the in-air hydrophone recordings.

The humpback breathing sounds recorded by in-air and underwater hydrophones during vertical drift deployment are similar to those shown in spectrograms of Watkins (1967) and Thompson et al. (1986). Although the humpback whale breathing sound signal duration for vertical drift deployment matches those in Watkins (1967), the measured frequency bandwidth of humpback wheezing blows in that publication did not match the bandwidth found here. This could be due to the lower sampling frequency (factor of ten smaller) used in Watkins (1967), leading to the inability to accurately compare signal energies above 4 kHz. Thompson et al. (1986) also analyzed humpback breathing sounds, classifying them as two different types; shrieks and trumpet-like horn blasts. After further review of the data recorded in the GSC, it was determined that the results align more with shrieks than with blasts, due to signal duration and bandwidth. The shrieks have an estimated duration of 1–1.5 s. This is roughly 1 s shorter than the recorded bandwidth of a single hydrophone in vertical drift deployment. However, an accurate comparison is difficult because Thompson et al. (1986) spectrograms have an unknown intensity scale. When reviewing the shriek bandwidth analyzed in Thompson et al. (1986), it appears the majority of the signal's intensity resides between 555 and 2000 Hz, but the spectrograms show the signal extending up to the 8 kHz upper spectrogram limit. Therefore, a comparison above 8 kHz cannot be made. The GSC is a major ecological region, residing between the Nantucket shoals and Georges bank providing a key migratory path for a myriad of marine wildlife species including the humpback whale.

The estimated source level distribution for humpback whale breathing sounds has a mean of 161 ± 4 dB re 1 μPa at 1 m and mode of 157 dB re 1 μPa at 1 m. These estimates are between 18 to 24 dB lower than the source level of 179–181 dB re 1 μPa at 1 m proposed in Thompson et al. (1986) for blowhole shrieks. Humpback whale social song and non-song vocalization source levels were also analyzed in Dunlop et al. (2008), Dunlop et al. (2013), and Dunlop et al. (2007) based on measurements along the east coast of Australia. A similar approach by assuming spherical spreading for transmission loss across the bandwidth of the signal was implemented to estimate source levels. Dunlop et al. (2013) provided root-mean square (RMS) source levels (SL_{RMS}) for a plethora of surface-sounds such as grunts and trumpetlike horn blasts. Dunlop et al. (2013) estimates have an average SL_{RMS} value of 158 dB re 1 μPa at 1 m for grunts and 159 dB re 1 μPa at 1 m for trumpetlike horn blasts, providing values close to the estimated source level distribution mean and mode obtained from our measurements here.

The frequency null/dip in the spectrogram [Fig. 5(a)] is a phenomenon observed in measurements of all underwater hydrophones of the subarray while deployed vertically. The strongest dip or null occurred at hydrophone 28 (depth of 5.245 m), and the effect decreases with increasing hydrophone depth. This phenomenon can be seen in Fig. 10, where a 10 Hz running average is applied to each of the underwater hydrophones used during vertical drift deployment.

Possible hypotheses for this null are investigated here, with the first being due to the Lloyd's mirror effect (LME). The LME was considered here since it was found in spectrograms of other marine mammal sounds, such as a series of fin whale 20 Hz pulses, with nulls observed at specific frequencies within the bandwidth of the fin whale calls (Pereira et al., 2016). The LME is a phenomenon that occurs due to

https://doi.org/10.1121/10.0036353

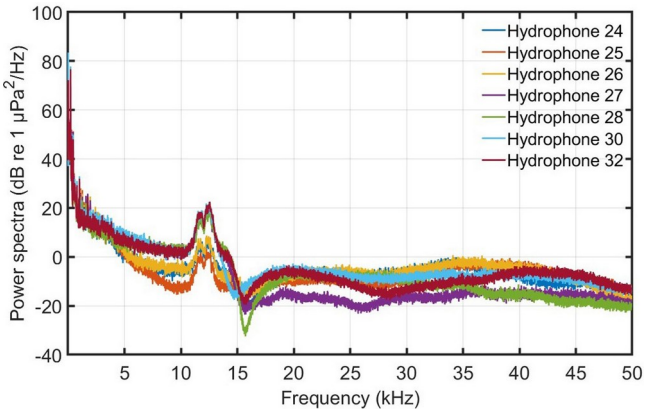

FIG. 10. Power spectrum of the 7 underwater hydrophones used during tical drift deployment with a 10 Hz running average applied on Septem 6, 2021 at 20:53 EDT, where the strongest dip occurs at hydrophone 28 (green).

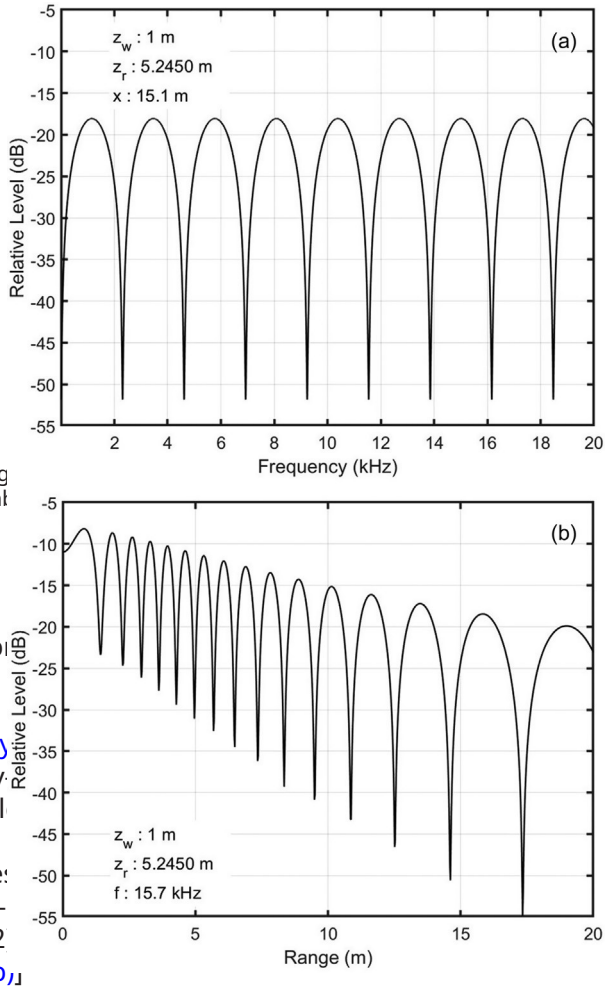

FIG. 11. Modeling Lloyd mirror effect (LME) to investigate potential impact on measured data for vertical drift deployment submerged hydrophone 28 on September 6, 2021 at 20:53 EDT. (a) The LME varying with acoustic frequency, and (b) the LME varying with range. Both these effects were not observed in the measured data, so LME cannot account for attenuation at 15.7 kHz in measured data shown in Fig. 5(a).

coherent interference of the acoustic wave fields reflected from sea-surface boundary with those from direct-path propagation at the receiver, causing nulls and peaks in the received signal intensity. Using the array geometry from Fig. 4 and equations from Audoly and Meyer (2017), Carey (2009), Jensen et al. (2011), and Norton et al. (1998), analysis was performed to determine the impact the LME would have on humpback breathing sound spectrograms. Two different scenarios were modeled and the acoustic intensities calculated: (1) varying frequency for a whale at fixed horizontal distance from receiver, as shown in Fig. 11(a), or (2) varying whale horizontal distance from receiver [Fig. 11(b)] at fixed frequency. From (1) it was determined that multiple nulls would occur at distinct frequencies including roughly 2.3, 4.6, 6.9, 9.2, 11.5, 13.8, 16.1, and 18.4 kHz [Fig. 11(a)] over the bandwidth of the humpback breathing sound, which was not observed. In (2), the interference pattern changes as a function of range so that the observed null at $f = 15.7$ kHz would not be consistently present, and the acoustic intensity at that frequency would vary from null to peak as a function of increasing whale range, which was also not observed in the data. Therefore, it is unlikely that the LME is creating the consistent frequency null centered at 15.7 kHz frequency observed here in the vertically deployed underwater hydrophone dataset.

The next hypothesis considered for causing the roughly 15.7 kHz frequency null/dip in observed humpback breathing sound spectrogram was the attenuation (Cho and Makris, 2020; Ratilal and Makris, 2005) from forward propagation through surface bubble layer caused by precipitation. Nystuen (1992) provides insights into rainfall rates and drop sizes associated with various categories of precipitation. Underwater noise measured in the presence of drizzle or light rainfall has a peak frequency of around 15 kHz, which coincides well with the frequency of the intensity null/dip measured here. During vertical drift deployments of the hydrophone subarray on the evening of September 6, 2021, no precipitation occurred during our measurement time interval at the GSC. With wind gusts of roughly 11.29 kt (5.8 m/s) and a wave height of 1.5 m, which corresponds to a Beaufort scale sea state level of 4, creating breaking waves that are a source of underwater bubbles. Breaking waves create bubbles of all sizes, where Deane and Stokes (2002) discusses their radius could range anywhere from 0.1 mm to more than 10 mm depending on the wave phase, where the majority of the noise created is below 1 kHz. With the wide range of bubbles created by the breaking waves, it is unlikely that they are the source of the 15.7 kHz centered frequency null observed here, since more frequencies over significantly wider bandwidth would be attenuated.

The most likely cause of the observed frequency null/dip in the measured spectrograms is attenuation from forward propagation through bubbles generated by humpback whales themselves, from surface breathing blows and sprays, underwater bubble clouds, swimming and other behavioral motions. It is hypothesized that the blow of a humpback whale creates sprays that hit the water surface

entraining air bubbles, similar in size to that of light rainfall or drizzle. These strong bubbles have natural oscillation frequencies near 15 kHz (Nystuen and Farmer, 1987; Nystuen and Ma, 2002; Nystuen et al., 1993; Pensieri et al., 2015; Scrimger et al., 1987), and likely also remove energy from any acoustic field propagating through the bubble cloud, due to the frequency null/dip. This approximation assumes that the bubble maintains a spherical shape, due to its small size (Medwin et al., 1992; Prosperetti et al., 1988). Humpback whales also expel large volume of air underwater, creating bubble walls or clouds often observed to coincide with feeding activities. Reidenberg and Laitman (2007a) state these bubble clouds can span 10 m in diameter and are comprised of individual bubbles, where Qing et al. (2019) records a mode radius of 0.019 mm, measured at-sea by Leighton et al. (2004). Based upon the mode radius of the bubbles created from the underwater cloud, and using the Minnaert (1933) relationship between bubble size to natural oscillation frequency [Eq. (7)], results in an approximate value of 171.7 kHz. Based upon that value, and the range in bubble sizes created from the cloud, it seems unlikely that this would create the observed frequency null/dip centered at 15.7 kHz. Given that the size of bubbles in the underwater cloud is small, one must determine whether the humpback surface spray creates bubbles of equal or similar size. Reidenberg and Laitman (2007a) determined that based upon the nasal construction of a humpback whale, it is unlikely that air released from surface blows produce similar minuscule bubbles characteristic of underwater bubble clouds.

It is important to discuss other humpback whale surface processes as potential origins for the formation of underwater bubbles. Clapham (2000) describes several behavioral displays such as surface (headfirst) and tail breaching, pectoral and tail surface slaps, and spyhopping. Given the visual accounts, and the humpback whales proximity being less than 30 m from the boat during the forty-minute vertical drift deployment, the only observed behavioral surface activity that occurred the evening of September 6 was spyhopping [Fig. 1(a)], which took place over 20-min prior to this analyzed data subset. Since the frequency null/dip was observed throughout the forty-minute vertical drift deployment, it is believed that the only mechanisms possible of creating the frequency dip/null is from the humpback whale surface spray or swimming motions occurring underwater.

It is difficult to estimate the exact droplet sizes associated with humpback whale spray, but they are most likely comprised of both small and large droplets with a maximum radius of approximately 2 mm (Butterworth, 2006). Given the variability in droplet sizes, it is important to consider the potential for Mesler entrainment. Mesler entrainment is the phenomenon where the impact of a single droplet creates the entrainment of numerous bubbles. The entrained bubbles radiate very small amounts of noise, and have a mean radius of 0.025 mm (Carroll and Mesler, 1981; Esmailizadeh and Mesler, 1986; Pumphrey and Elmore, 1990). Pumphrey and Elmore (1990) describe the inconsistencies in the amount of bubbles entrained for even a consistent environment (clean fresh water, constant temperature, and vertical drop trajectory), and we must note that temperature, liquid cleanliness, and drop trajectory associated with humpback whale spray presumably varies. Due to the lack of literature surrounding humpback whale spray droplets, we will be using the approximations put forth by Pumphrey and Elmore (1990), and must note the uncertainties in drop trajectory and biological contaminants in the spray. Although Mesler entrainment is inconsistent as described previously, it is most common when the drop is at a low impact velocity. By, upon a drop size diameter ranging from 0.8 to 1.1 mm (light rainfall/drizzle), and the third-degree regression terminal velocity formula from Dingle and Lee (1972), 0.8 and 1.1 mm drop diameters have terminal velocities of 3.28 and 4.35 m/s, respectively. In order to determine if the humpback whale spray drops produce regular entrainment, as first described in Pumphrey and Walton (1988), we must determine the distance needed for these drops to reach terminal velocity, and in-turn produce underwater sound (Pumphrey and Elmore, 1990). Humpback whales surface breathing sprays typically reach heights of 2–3 m (Leatherwood et al., 1982), therefore, based upon these drop sizes, they need to reach terminal velocities prior to a distance of 2 m. With the known terminal velocities from Dingle and Lee (1972), we can next estimate the distance needed to reach that velocity in air,

$$d = \frac{v_t^2}{2g}; \tag{6}$$

where d is the distance it takes to reach terminal velocity, g is the acceleration due to gravity, and v_t is the constant terminal velocity of the droplet. Using this equation, we arrive at an approximate distance of 0.55 m for a 0.8 mm droplet, and 0.96 m for a 1.1 mm droplet. Based upon these findings and assumptions, it is concluded that the spray from the humpback whales have the possibility of reaching terminal velocity, and therefore could produce regular entrainment.

We next infer bubble sizes that would lead to natural frequencies between 15 and 16 kHz and subsequent attenuation in the forward propagated acoustic field at that frequency. All 76 data files on the evening of September 6, 2021 from 20:29 EDT to 21:09 EDT are analyzed, and spectra from hydrophone 28 calculated with a 10 Hz running average and overlain in Fig. 12(a), along with the mean spectrum. The precise frequency of occurrence of the intensity null/dip varied between individual spectra ranging from 15.55 to 15.92 kHz with a mean of 15.72 kHz. The bubbles pulsating at these frequencies have varying radii ranging from 0.2048 to 0.2098 mm and mean of 0.2074 mm, as tabulated in Table II. It should be noted that larger bubbles oscillate at lower frequencies compared to smaller bubbles, the transformation from bubble radius to oscillation frequency is inverse and nonlinear. In order to accurately characterize and quantify the broadband dip, it is necessary to obtain the average power spectrum in the absence of echosounder

https://doi.org/10.1121/10.0036353

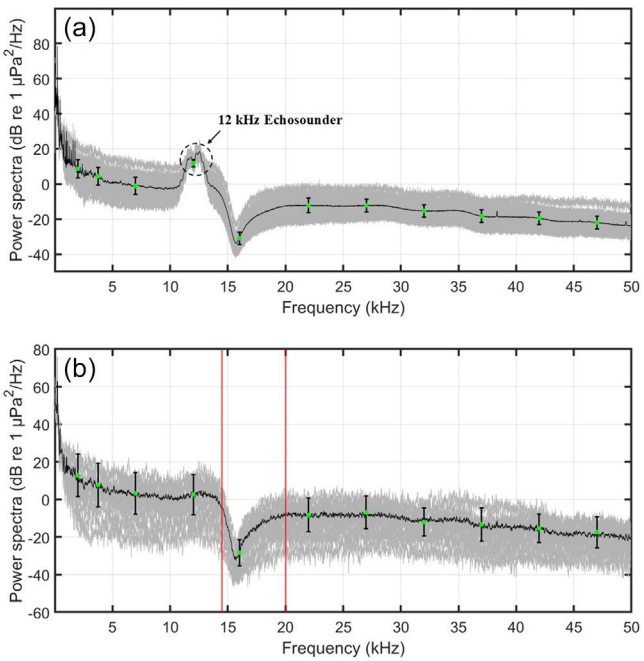

FIG. 12. These results are obtained from submerged hydrophone 28 measurements during vertical drift deployment on September 6, 2021 from 20:29 EDT to 21:09 EDT containing humpback whale breathing sounds. (a) Power spectrum of 76 data files (overlain in gray) and average spectrum (in black). (b) Power spectrum of 20 data files (overlain in gray), each with absence of 12 kHz echosounder signals, and average spectrum (in black). The error bars indicate spectrum standard deviation values at those particular frequencies.

signals. Out of the total 76 data files analyzed, 20 of them were recorded in the absence of echosounder signals. This subset of echosounder-free recordings are analyzed and spectra with 50 Hz running average overlain in Fig. 12(b), along with the mean spectrum.

A pulsating air bubble has a sharp sub-resonance rise and a more gradual super-resonance fall (Gong et al., 201 Medwin, 1977; Pumphrey and Crum, 1990; Pumphrey et al., 1989) in both acoustic scattered and natural oscillation intensities. Consequently, the attenuation caused by pulsating bubble will show a similar pattern with a sharpe pre-resonance attenuation dip and a more gradual post-resonance attenuation rise. Here, the intensity dip/null in Fig. 12(b) is best approximated as a band-stop filter with center frequency 15.7 kHz, and bandwidth 5.5 kHz [marked by red vertical lines in Fig. 12(b)]. The pre-resonance dip has a sharp roll-off around 89 dB/octave beginning at 14.5 kHz, equivalent to a 15th order filter. The post-resonance rise is more gradual with slope of around 55 dB/octave extending out to 20 kHz, equivalent to a 9th order filter. The pre- and post-dip intensity variations provide further confirmation that the null or attenuation is caused by bubble oscillation.

The frequency dip min, max and mean values, along with standard deviation estimated from measured spectra are tabulated in Table II with histogram shown in Fig. 13(a). The 3 dB null bandwidths are calculated from each spectra

TABLE II. Statistics of measured dip frequency values, measured 3 dB dip bandwidths, and corresponding bubble radii with natural oscillation frequencies matching corresponding dip frequencies. These results are based on analysis of 76 data files from submerged hydrophone 28 containing humpback whale breathing sounds during vertical drift deployment on September 6, 2021 from 20:29 EDT to 21:09 EDT, as well as modeling entrained air bubble natural frequency. Blue (min dip frequency, max bubble radius) and brown (max dip frequency, min bubble radius) characters show the inverse and nonlinear transformation between bubble radius and dip frequency value.

Parameter	Minimum	Mean	Maximum	Standard deviation
Dip frequency (kHz)	15.548	15.723	15.923	$65.354\ 10^{-3}$
3 dB dip bandwidth (Hz)	85.734	285.651	503.807	113.652
Bubble radius (mm)	0.2048	0.2074	0.2098	$8.61\ 10^{-4}$

as the 3 dB higher intensity from the null, where large variation can occur as seen in Table II and Fig. 13(b). The corresponding bubble radius distribution that would lead to bubble resonances at the experimentally measured dip frequencies are also tabulated and shown in Fig. 13(c). These

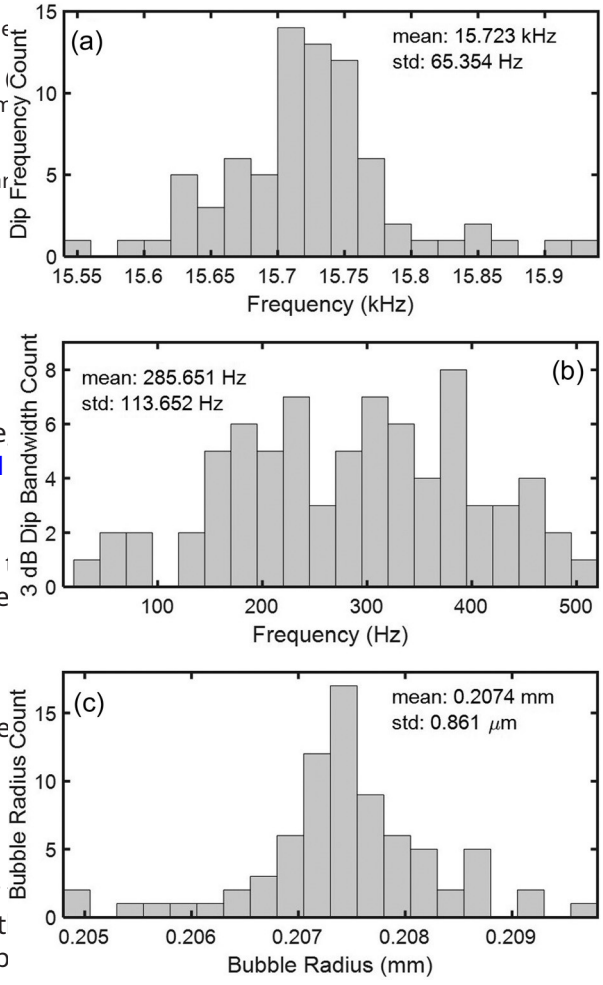

FIG. 13. Results from analysis and modeling based on 76 data files of submerged hydrophone 28 containing humpback whale breathing sounds during vertical drift deployment on September 6, 2021 from 20:29 EDT to 21:09 EDT. Histograms of (a) measured dip frequency; (b) measured 3 dB dip bandwidth; (c) inferred bubble radius for corresponding dip frequency.

results indicate that the bubble size distribution and densities are varying in time leading to variations in dip frequenci and dip bandwidth extent.

Here, the relationship between natural oscillation frequency and bubble radius used to infer the results in Ta II follow Minnaert (1933),

$$f_0 = \frac{1}{2\pi R_0}\sqrt{\frac{3cP_0}{\rho_0}}; \quad (7)$$

where f_0 is the natural oscillation frequency, R_0 is the bubble radius, c is the ratio of specific heats, P_0 is the static pressure, and ρ_0 is the density of seawater. The following values were assumed for calculating the relationship at the water surface: $c = 1.40$; $P_0 = 101\,325$ Pa, and $\rho_0 = 1030$ kg/m^3. These values correspond to bubble radius sizes in water at sea level shown in Medwin (1977).

The damping constants along with scattering, extinction, and absorption cross-sections are next approximated to provide insight into the dominant mechanism for sound attenuation from the pulsating air bubbles. The total damping constant, d, associated with the pulsating air bubbles is

$$d = d_{th} + d_{ac} + d_{vis}; \quad (8)$$

where d_{th} is thermal damping, d_{ac} is acoustic radiation damping, and d_{vis} is the viscous damping. These damping coefficients are plotted in Fig. 14(a) as a function of frequency for bubble radius $R_0 = 0.2074$ mm using the formulation of Devin (1959). Both viscous and thermal damping increase with frequency, with the exception of acoustic damping, which remains nearly constant. The scattering, σ_s, extinction, σ_e, and absorption, σ_a, cross-sections are determined following the formulation in Ainslie and Leighton (2011),

$$\sigma_s = \frac{4\pi R_0^2}{\left(\frac{x_0^2}{x^2} - 1\right)^2 + d^2}; \quad (9)$$

$$\sigma_e = \frac{d}{x R_0/c}\,\sigma_s; \quad (10)$$

$$\sigma_a = \sigma_e - \sigma_s; \quad (11)$$

where x_0 is the bubble resonance frequency. These equations produce the output as shown in Fig. 14(b), with peak cross-sections occurring at about 15.7 kHz. The leading cause of extinction or attenuation at the bubble resonance of the acoustic intensity is absorption.

To validate the hypothesis that the null/dip frequency of 15.7 kHz originates from humpback whale spray, droplet samples at sea would need to be captured. This scenario should then be recreated in the laboratory where the droplets fall at their appropriate impact speed into saltwater, to determine if they have natural frequencies ranging between 15 and 16 kHz. Until then, it remains a hypothesis that the

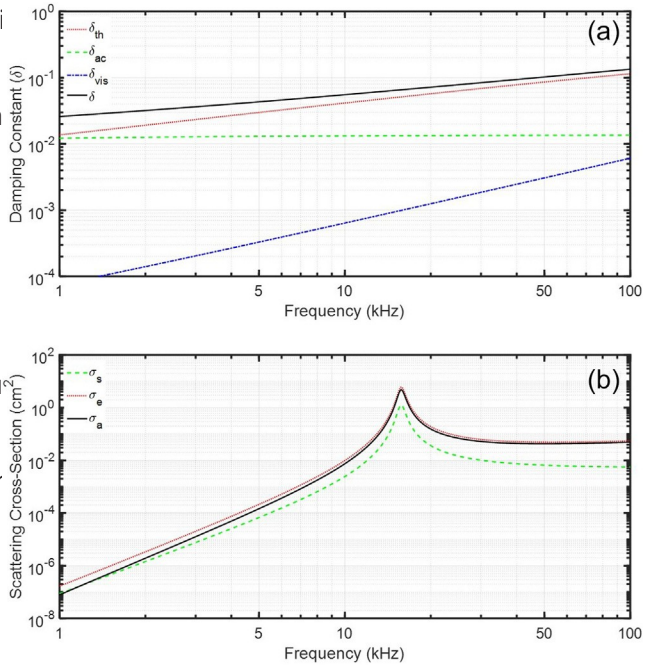

FIG. 14. (a) Damping constant, d, varying with frequency for a bubble radius, R_0 of 0.2074 mm taken from Table II. Dotted line (red): thermal damping, d_{th}; dashed line (green): acoustic damping, d_{ac}; dot-dashed line (blue): viscous damping, d_{vis}; solid line (black) total damping d [after Devin, Jr. (1959)]. (b) Shows the different cross-sections, where their peak is at resonance. Dashed line (green): scattering; Dotted line (red): extinction; solid black line: absorption.

humpback whale spray is the reason for the 15.7 kHz centered broadband frequency dip/null.

V. CONCLUSIONS

Breathing sounds from humpback whales in the Great South Channel region of the U.S. Northeast continental shelf have been measured and analyzed based on data acquired with subapertures of a coherent hydrophone array during an experiment in Fall 2021. Video recordings and visual sightings enabled humpback breathing sounds to be coregistered with those measured on the hydrophone subarray deployed in both vertical drift and horizontal tow. A combination of time-series, spectrogram and PSD analysis was conducted to understand and characterize measured humpback breathing sound signals in both in-air and underwater, including frequency ranges, bandwidths, and signal durations. This analysis sheds more light into sounds humpback whales make both above and below the water surface, as well as how these sounds are perceived in air and underwater.

Here, the underwater recorded humpback breathing sounds were used to infer humpback whale ranges from the vertical hydrophone subarray by employing near-field nonlinear time of arrival analysis on individual hydrophone elements. The sequence of range estimates were then applied to estimate humpback whale breathing sound underwater source level distribution which resulted in a mean of 161 ± 4 dB re 1 μPa at 1 m and most probable value of

157 dB re 1 μPa at 1 m. Furthermore, we discovered an intensity reduction or dip in the measured spectra of the vertical hydrophone subarray while deployed in the vicinity of humpback whale breathing activity. The broadband dip/null centered at 15.7 kHz is most likely caused by attenuation from pulsating air bubbles, probably generated by the humpback whales themselves through movement, breathing, or underwater bubble clouds.

SUPPLEMENTARY MATERIAL

See the supplementary material for videos and spectrograms of humpback whale breathing sounds.

ACKNOWLEDGMENTS

This research was funded by United States Office of Naval Research Grant Nos. N00014-23-1-2327 and N00014-20-1-2026, and United States National Science Foundation Grant Nos. OCE-2219953, TI-2345791, and OCE-1736749.

AUTHOR DECLARATIONS

Conflict of Interest

The authors have no conflicts to disclose.

DATA AVAILABILITY

The data that support the findings of this study are available from the corresponding author upon reasonable request.

Ainslie, M. A., and Leighton, T. G. (2011). "Review of scattering and extinction cross-sections, damping factors, and resonance frequencies of a spherical gas bubble," J. Acoust. Soc. Am. 130(5), 3184–3208.
Anagnostou, M. N., Nystuen, J. A., Anagnostou, E. N., Nikolopoulos, E. I., and Amitai, E. (2008). "Evaluation of underwater rainfall measurements during the Ionian Sea rainfall experiment," IEEE Trans. Geosci. Remote Sens. 46(10), 2936–2946.
Au, W. W., Pack, A. A., Lammers, M. O., Herman, L. M., Deakos, M. H., and Andrews, K. (2006). "Acoustic properties of humpback whale songs," J. Acoust. Soc. Am. 120(2), 1103–1110.
Audoly, C., and Meyer, V. (2017). "Measurement of radiated noise from surface ships—Influence of the sea surface reflection coefficient on the Lloyd's mirror effect," in Proceedings of ACOUSTICS 2017, Perth, Australia (November 19–22).
Auvinen, M. F., Barclay, D. R., and Coffin, M. E. (2020). "Performance of a passive acoustic linear array in a tidal channel," IEEE J. Oceanic Eng. 45(4), 1564–1573.
Barclay, D. R., and Buckingham, M. J. (2013a). "The depth-dependence of rain noise in the Philippine Sea," J. Acoust. Soc. Am. 133(5), 2576–2585.
Barclay, D. R., and Buckingham, M. J. (2013b). "Depth dependence of wind-driven broadband ambient noise in the Philippine Sea," J. Acoust. Soc. Am. 133(1), 62–71.
Butterworth, A. (2006). "Thermography of respiratory activity in Cetacea," in Proceedings of the International Whaling Commission IWC/58/WKM and AWI 24 (5.2).
Carey, W. M. (2009). "Lloyd's mirror-image interference effects," Acoust. Today 5(2), 14–20.
Carroll, K., and Mesler, R. (1981). "Part II: Bubble entrainment by drop-formed vortex rings," AIChE J. 27(5), 853–856.
Cato, D. H. (1978). "Marine biological choruses observed in tropical waters near Australia," J. Acoust. Soc. Am. 64(3), 736–743.
Cato, D. H. (1992). "The biological contribution to the ambient noise in waters near Australia," Acoust. Australia 20, 76–80.
Cazau, D., Adam, O., Aubin, T., Laitman, J. T., and Reidenberg, J. S. (2016). "A study of vocal nonlinearities in humpback whale songs: From production mechanisms to acoustic analysis," Sci. Rep. 6(1), 31660.
Cho, B., and Makris, N. C. (2020). "Predicting the effects of random ocean dynamic processes on underwater acoustic sensing and communication," Sci. Rep. 10(1), 4525.
Clapham, P. J. (2000). "The humpback whale," in Cetacean Societies: Field Studies of Dolphins and Whales, edited by J. Mann, R. C. Connor, P. L. Tyack, and H. Whitehead (University of Chicago Press, Chicago, IL), Chap. 7, pp. 173–175.
Damien, J., Adam, O., Cazau, D., White, P., Laitman, J. T., and Reidenberg, J. S. (2019). "Anatomy and functional morphology of the mysticete rorqual whale larynx: Phonation positions of the U-fold," Anatomical Rec. 302(5), 703–717.
Deane, G. B., and Stokes, M. D. (2002). "Scale dependence of bubble creation mechanisms in breaking waves," Nature 418(6900), 839–844.
Devin, C., Jr. (1959). "Survey of thermal, radiation, and viscous damping of pulsating air bubbles in water," J. Acoust. Soc. Am. 31(12), 1654–1667.
Dingle, N., and Lee, Y. (1972). "Terminal fallspeeds of raindrops," J. Appl. Meteor. 11(5), 877–879.
Dunlop, R. A., Cato, D. H., and Noad, M. J. (2008). "Non-song acoustic communication in migrating humpback whales (Megaptera novaeangliae)," Mar. Mammal Sci. 24(3), 613–629.
Dunlop, R. A., Cato, D. H., Noad, M. J., and Stokes, D. M. (2013). "Source levels of social sounds in migrating humpback whales (Megaptera novaeangliae)," J. Acoust. Soc. Am. 134(1), 706–714.
Dunlop, R. A., Noad, M. J., Cato, D. H., and Stokes, D. (2007). "The social vocalization repertoire of east Australian migrating humpback whales (Megaptera novaeangliae)," J. Acoust. Soc. Am. 122(5), 2893–2905.
Erbe, C. (2002). "Hearing abilities of baleen whales," Defence Research and Development Canada Atlantic, Report CR 65.
Esmailizadeh, L., and Mesler, R. (1986). "Bubble entrainment with drops," J. Colloid Interface Sci. 110(2), 561–574.
Francois, R., and Garrison, G. (1982). "Sound absorption based on ocean measurements: Part I: Pure water and magnesium sulfate contributions," J. Acoust. Soc. Am. 72(3), 896–907.
Gandilhon, N., Adam, O., Cazau, D., Laitman, J. T., and Reidenberg, J. S. (2015). "Two new theoretical roles of the laryngeal sac of humpback whales," Mar. Mammal Sci. 31(2), 774–781.
Garcia, H. A., Couture, T., Galor, A., Topple, J. M., Huang, W., Tiwari, D., and Ratilal, P. (2020). "Comparing performances of five distinct automatic classifiers for fin whale vocalizations in beamformed spectrograms of coherent hydrophone array," Remote Sens. 12(2), 326.
Garcia, H. A., Zhu, C., Schinault, M. E., Kaplan, A. I., Handegard, N. O., Godø, O. R., Ahonen, H., Makris, N. C., Wang, D., Huang, W., and Ratilal, P. (2019). "Temporal–spatial, spectral, and source level distributions of fin whale vocalizations in the Norwegian sea observed with a coherent hydrophone array," ICES J. Mar. Sci. 76(1), 268–283.
Godin, O. (2007). "Transmission of low-frequency sound through the water-to-air interface," Acoust. Phys. 53, 305–312.
Godin, O. A. (2006). "Anomalous transparency of water-air interface for low-frequency sound," Phys. Rev. Lett. 97(16), 164301.
Godin, O. A. (2008a). "Low-frequency sound transmission through a gas–liquid interface," J. Acoust. Soc. Am. 123(4), 1866–1879.
Godin, O. A. (2008b). "Sound transmission through water–air interfaces: New insights into an old problem," Contemp. Phys. 49(2), 105–123.
Gong, Z., Andrews, M., Jagannathan, S., Patel, R., Jech, J. M., Makris, N. C., and Ratilal, P. (2010). "Low-frequency target strength and abundance of shoaling Atlantic herring (Clupea harengus) in the Gulf of Maine during the ocean acoustic waveguide remote sensing 2006 experiment," J. Acoust. Soc. Am. 127(1), 104–123.
Heerton, T. W., Oline, A., Hauser, N., Khan, T. M., Laute, A., Stoller, A., Tison, K., and Zawar-Reza, P. (2017). "Thermal imaging and biometrical thermography of humpback whales," Front. Mar. Sci. 4, 424.
Huang, W., Wang, D., and Ratilal, P. (2016). "Diel and spatial dependence of humpback song and non-song vocalizations in fish spawning ground," Remote Sens. 8(9), 712.
Jensen, F. B., Kuperman, W. A., Porter, M. B., Schmidt, H., and Tolstoy, A. (2011). Computational Ocean Acoustics (Springer, Berlin, Germany), Chap. 1.4.2.

Krogh, A. (1934). "Physiology of the blue whale," Nature 133(3365), 635–637.
Leatherwood, S., Reeves, R. R., Perrin, W. F., Evans, W. E., and Hobbs, L. J. (1982). "Whales, dolphins, and porpoises of the eastern north pacific and adjacent arctic waters: A guide to their identification," NOAA Technical Report NMFS Circular 444.
Leighton, T., Meers, S., and White, P. (2004). "Propagation through nonlinear time-dependent bubble clouds and the estimation of bubble population distributions from measured acoustic characteristics," Proc. Soc. London A 460(2049), 2521–2550.
Ma, B. B., Dushaw, B. D., and Howe, B. M. (2022). "Rainfall at sea: Using the underwater sounds of raindrops as a rain gauge for weather and climate," Acoust. Today 18(2), 62–71.
Ma, B. B., and Nystuen, J. A. (2005). "Passive acoustic detection and measurement of rainfall at sea," J. Atmos. Oceanic Technol. 22(8), 1225–1248.
McDonald, B. E., and Calvo, D. C. (2007). "Enhanced sound transmission from water to air at low frequencies," J. Acoust. Soc. Am. 122(6), 3159–3161.
Medwin, H. (1977). "Counting bubbles acoustically: A review," Ultrasonics 15(1), 7–13.
Medwin, H., Nystuen, J. A., Jacobus, P. W., Ostwald, L. H., and Snyder, D. E. (1992). "The anatomy of underwater rain noise," J. Acoust. Soc. Am. 92(3), 1613–1623.
Minnaert, M. (1933). "XVI. On musical air-bubbles and the sounds of running water," London, Edinburgh, Dublin Philos. Mag. J. Sci. 16(104), 235–248.
Mohebbi-Kalkhoran, H., Schinault, M., Makris, N. C., and Ratilal, P. (2022). "Integrated computing system for real-time data processing, storage and communication with large aperture 160-element coherent hydrophone array," in Oceans 2022, Hampton Roads, pp. 1–9.
Noad, M. J., Cato, D. H., Bryden, M. M., Jenner, M.-N., and Jenner, K. C. S. (2000). "Cultural revolution in whale songs," Nature 408(6812), 537–537.
Norton, G. V., Novarini, J. C., and Keiffer, R. S. (1998). "Modeling the propagation from a horizontally directed high-frequency source in shallow water in the presence of bubble clouds and sea surface roughness," J. Acoust. Soc. Am. 103(6), 3256–3267.
Nystuen, J. A. (1992). "Rainfall measurement using passive underwater acoustical remote sensing," in OCEANS 92 Proceedings@ m_Mastering the Oceans Through Technology (IEEE, Piscataway, NJ), Vol. 1, pp. 508–513.
Nystuen, J. A., and Farmer, D. M. (1987). "The influence of wind on the underwater sound generated by light rain," J. Acoust. Soc. Am. 82(1), 270–274.
Nystuen, J. A., and Ma, B. (2002). "Using ambient sound to passively monitor sea surface processes," in Proceedings of the Sixth Pan Ocean Remote Sensing Conference (PORSEC) (PORSEC Association, New York), pp. 9–14.
Nystuen, J. A., McGlothin, C. C., and Cook, M. S. (1993). "The underwater sound generated by heavy rainfall," J. Acoust. Soc. Am. 93(6), 3169–3177.
Payne, R. S., and McVay, S. (1971). "Songs of humpback whales: Humpbacks emit sounds in long, predictable patterns ranging over frequencies audible to humans," Science 173(3997), 585–597.
Pensieri, S., Bozzano, R., Nystuen, J. A., Anagnostou, E. N., Anagnostou, M. N., and Bechini, R. (2015). "Underwater acoustic measurements to estimate wind and rainfall in the Mediterranean Sea," Adv. Meteorol. 2015(1), 612512.
Pereira, A., Harris, D., Tyack, P., and Matias, L. (2016). "Lloyd's mirror effect in fin whale calls and its use to infer the depth of vocalizing animals," Proc. Mtgs. Acoust. 27, 070002.
Prosperetti, A., Crum, L. A., and Commander, K. W. (1988). "Nonlinear bubble dynamics," J. Acoust. Soc. Am. 83(2), 502–514.
Pumphrey, H. C., and Crum, L. (1990). "Free oscillations of near-surface bubbles as a source of the underwater noise of rain," J. Acoust. Soc. Am. 87(1), 142–148.
Pumphrey, H. C., Crum, L., and Bjørnø, L. (1989). "Underwater sound produced by individual drop impacts and rainfall," J. Acoust. Soc. Am. 85(4), 1518–1526.
Pumphrey, H. C., and Elmore, P. A. (1990). "The entrainment of bubbles by drop impacts," J. Fluid Mech. 220, 539–567.
Pumphrey, H. C., and Walton, A. J. (1988). "Experimental study of the sound emitted by water drops impacting on a water surface," Eur. J. Phys. 9(3), 225.
Qiang, X., White, P. R., Leighton, T. G., Liu, S., Qiao, G., and Zhang, Y. (2019). "Three-dimensional finite element simulation of acoustic propagation in spiral bubble net of humpback whale," J. Acoust. Soc. Am. 146(3), 1982–1995.
Radermacher, M. K., Schinault, M. E., Seri, S. G., and Ratilal, P. (2022). "Research and design for the power hierarchy of a 160-element linear towable ocean acoustic coherent hydrophone array," in Oceans 2022, Hampton Roads, pp. 1–7.
Ratilal, P., and Makris, N. C. (2005). "Mean and covariance of the forward field propagated through a stratified ocean waveguide with three-dimensional random inhomogeneities," J. Acoust. Soc. Am. 118(6), 3532–3559.
Ratilal, P., Seri, S. G., Mohebbi-Kalkhoran, H., Zhu, C., Schinault, M., Radermacher, M., and Makris, N. C. (2022). "Continental shelf-scale passive ocean acoustic waveguide remote sensing of marine ecosystems, dynamics and directional soundscapes: Sensing whales, fish, ships and other sound producers in near real-time," in Oceans 2022, Hampton Roads, pp. 1–7.
Reidenberg, J. S., and Laitman, J. T. (2007a). "Blowing bubbles: An aquatic adaptation that risks protection of the respiratory tract in humpback whales (Megaptera novaeangliae)," Anat. Rec. 290(6), 569–580.
Reidenberg, J. S., and Laitman, J. T. (2007b). "Discovery of a low frequency sound source in Mysticeti (baleen whales): Anatomical establishment of a vocal fold homolog," Anat. Rec. 290(6), 745–759.
Schinault, M. E., Seri, S. G., Radermacher, M. K., Mohebbi-Kalkhoran, H., Zhu, C., Makris, N.C., and Ratilal, P. (2022). "Development of a large-aperture 160-element coherent hydrophone array system for instantaneous wide area ocean acoustic sensing," in Oceans 2022, Hampton Roads, pp. 1–9.
Scrimger, J. A., Evans, D. J., McBean, G. A., Farmer, D. M., and Kerman, B. R. (1987). "Underwater noise due to rain, hail, and snow," J. Acoust. Soc. Am. 81(1), 79–86.
Seri, S. G. (2024). "Advancing passive ocean acoustic waveguide remote sensing for detection of fish sounds, seismo-acoustic airgun signals and marine mammal vocalizations," Ph.D. thesis, Northeastern University, Boston, MA.
Seri, S. G., Schinault, M. E., Penna, S. M., Zhu, C., Sivle, L. D., de Jong, K., Handegard, N. O., and Ratilal, P. (2023). "Characterizing coastal cod vocalization using a towed hydrophone array," ICES J. Mar. Sci. 80(6), 1727–1745.
Thompson, P. O., Cummings, W. C., and Ha, S. J. (1986). "Sounds, source levels, and associated behavior of humpback whales, southeast Alaska," J. Acoust. Soc. Am. 80(3), 735–740.
Urick, R. J. (1983). Principles of Underwater Sound, 3rd ed. (Peninsula Publishing, Westport, CT), Chap. 8.9, pp. 249–254.
Wang, D., Garcia, H., Huang, W., Tran, D., Jain, A., Gong, Z., Jech, J. M., Godø, O. R., Makris, N. C., and Ratilal, P. (2016). "Vast assembly of vocal marine mammals from diverse species on fish spawning ground," Nature 531(7594), 366–370.
Watkins, W. A. (1967). "Air-borne sounds of the humpback whale, Megaptera novaeangliae," J. Mammal. 48(4), 573–578.
Wilson, J. D., and Makris, N. C. (2006). "Ocean acoustic hurricane classification," J. Acoust. Soc. Am. 119(1), 168–181.
Wilson, J. D., and Makris, N. C. (2008). "Quantifying hurricane destructive power, wind speed, and air-sea material exchange with natural undersea sound," Geophys. Res. Lett. 35(10), L10603, https://doi.org/10.1029/2008GL033200.
Winn, H., and Winn, L. (1978). "The song of the humpback whale Megaptera novaeangliae in the west indies," Mar. Biol. 47, 97–114.
Yeates, L. C., Borras, E., Cumeras, R., and Davis, C. E. (2020). "Breath analysis in marine mammals," in Breathborne Biomarkers and the Human Volatilome (Elsevier, Amsterdam), pp. 461–472.
Zhu, C., Seri, S. G., Mohebbi-Kalkhoran, H., and Ratilal, P. (2020). "Long-range automatic detection, acoustic signature characterization and bearing-time estimation of multiple ships with coherent hydrophone array," Remote Sens. 12(22), 3731.